Multifold Weyl semimetals under irradiation: The particularity of singlet Weyl points

Mou Yang,* Hao-Bin Ding, Ming-Xun Deng, and Rui-Qiang Wang
Guangdong Basic Research Center of Excellence for Structure and Fundamental Interactions of Matter, Guangdong Provincial Key Laboratory of Quantum Engineering and Quantum Materials, School of Physics, South China Normal University, Guangzhou 510006, China

(Received 20 January 2024; accepted 26 March 2024; published 15 April 2024)

We investigate the topological phases of Weyl semimetals possessing a pair of multifold (N-fold) Weyl points (WPs) irradiated by an off-resonant circularly polarized light in the frame of Floquet theory. The irradiation splits each N-fold WP into two singlet WPs and one residual WP of $N-2$ fold in k space. When the irradiation intensity increases, the two singlet WP pairs move faster and are gapped out first; therefore, a phase transition from N-fold to $(N-2)$-fold Weyl semimetal occurs. The pair of remaining $(N-2)$-fold WPs are annihilated later and a sequential phase transition to insulator happens. The irradiation influences the system by means of two mechanisms—the time average of the perturbation and the emission and reabsorption of photons, with the latter usually regarded as responsible for the phase transitions of matter and the former sometimes omitted due to its trivial effect. However, we find that these phase transitions are caused by the former, not by the latter, and the latter only affects how the WPs in the same pair approach each other, except for the case of $N=1$ in which both mechanisms take effect. The most common Weyl semimetal, say $N=1$, has the most special response. The irradiation can induce not only the transition from Weyl semimetal to insulator, but also the inverse transition, while the latter cannot happen in Weyl semimetals with $N \geqslant 2$.

DOI: 10.1103/PhysRevB.109.165126

I. INTRODUCTION

Weyl semimetal is a kind of three-dimensional (3D) topological material in which the conduction and valence bands touch at pairs of points named Weyl points (WPs) [1–3]. The Weyl semimetal hosts topologically protected Fermi arcs that consist of surface states and connect the WPs in one pair. The WPs with opposite chiralities act as magnetic monopoles in momentum space and the nature of WP chirality is the physical origination of many intriguing effects such as the chiral anomaly, planar Hall effect, and 3D Hall effect [1,2]. Besides the most common Weyl semimetals with linear dispersion, the multifold Weyl semimetals possess multifold WPs that are formed by merging two and more WPs with the same chirality so that a multifold WP carries multitopological charge (Chern number greater than one) [4–7]. The multifold Weyl semimetals have a mix of linear and higher-order dispersions and host multiple Fermi arcs on the surface Brillouin zone. Due to the fantasy of Weyl semimetals, the interest on Weyl quasiparticles in solid media is extended to cold atoms [8], photonic crystals [9–11], and phononic lattices [12,13].

Normally, topological phases of matter are very limited, so creating or engineering topological materials is highly desired in the society of condensed matter physics. In the ages of the graphene rising [14,15], it was found that the periodic perturbation of light can turn graphene into a topological insulator and new edge states correspondingly appear [16–22], which opens up a pathway towards Floquet topological physics due to the high tunability of light fields [23–27]. The light irradiation can break the time-reversal symmetry and add a mass term to the Hamiltonian to induce the phase transitions of matter [28–31]. In the past decade, great progress has been made in exploring various Floquet topological states driven by optical perturbations. The phase transitions between Weyl semimetal and Dirac material [31–33], nodal line medium [34–38], topological insulator [39–42], high-order topological material [43,44], and normal insulator [45] were found to be induced by circularly polarized light illumination. The Floquet-Bloch states [46,47] and the quantum anomalous Hall current in Floquet topological insulators [48–50] were observed experimentally. On the march of researching singlet Weyl semimetals, the physics of multifold Weyl semimetals under periodic perturbation is placed on the table. It was reported that the multifold Weyl phase can be induced by irradiation on crossing-nodal line semimetals [51,52]. When the lattice hoppings are changed alternatively between difference choices, in which each choice of hopping leads to a Weyl semimetal of a different fold, the hybrid multifold Weyl phase appears [53].

Though the phases of matter of singlet Weyl semimetal under irradiation were studied extensively, what happens in multifold Weyl semimetals is insufficient by now. In this paper, we investigate the splitting and moving of WPs of multifold (N-fold) Weyl semimetals irradiated by an off-resonant circularly polarized light. We first review the off-resonant effect in the language of Floquet theory and formulate generally the effective Hamiltonian that can reflect the phase transitions of matter. We figure out two mechanisms—the time average of the perturbation and the emission and reabsorption of photons—to renormalize the Hamiltonian of the system. The latter mechanism is usually regarded to induce

*yang.mou@hotmail.com

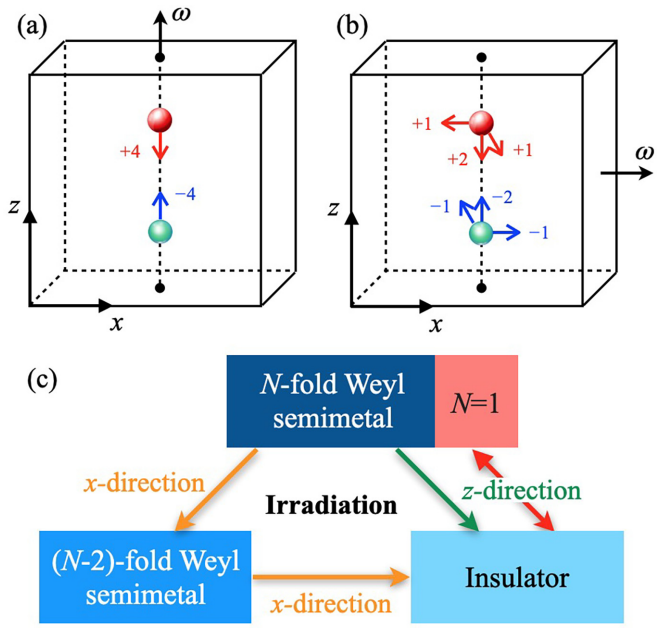

FIG. 1. (a),(b) Sketches of Weyl point (WP) splitting and moving in k space when the multifold ($N = 4$) Weyl semimetal is irradiated by a circularly polarized light in a different direction. The split WP pairs draw trajectories in the k_x-k_z plane (see Fig. 3) when the irradiation intensity increases. (c) Transitions between phases of matter.

the phase transitions of matter and so the former is omitted in some literatures [35,54]. However, we find that the former, not the latter, is the main mechanism for these phase transitions. Following, we apply the deduced Hamiltonian to the multifold Weyl semimetals and research the irradiation effect when the light illuminates in different directions. Finally, we discuss our calculation details and summarize our results.

The main conclusions are visually presented in Fig. 1. When the irradiation is applied along the direction of the WP connection (the line stemmed from the negative chiral WP to the positive one) and increases, the WPs for $N \geqslant 2$ approach each other straightly and the WP connection is shortened as Fig. 1(a) shows. When the light illuminates perpendicularly to the WP connection, the irradiation direction and the WP connection span a plane. Under the illumination, each multifold WP is split into two singlet WPs and one WP of $(N-2)$ fold and these WPs are scattered and move in the spanned plane, as shown in Fig. 1(b). The singlet WP pairs are gapped out first, the remaining WP pair are annihilated later, and the material undergoes two phase transitions of matter—the Weyl semimetal of N fold to that of $(N-2)$ fold to insulator. Figure 1(c) shows the possible matter phases of the multifold Weyl semimetal and the transitions between them. The irradiation along the WP connection causes direct transition from N-fold semimetal to insulator, while the perpendicular irradiation has to first drive the medium to an intermediate phase, $(N-2)$-fold Weyl semimetal, before turning it into an insulator. All the phase transitions are unidirectional except for the $N = 1$ case. This is because the response of the Weyl semimetal for $N = 1$ is quite different from $N \geqslant 2$ cases. When $N = 1$, the irradiation causes the WP connection to be shortened or elongated, depending on the irradiation intensity and orientation. The ability of shortening and elongation under the irradiation means that the phase transition from Weyl semimetal to insulator can be realized by canceling out the WP pair and the reverse phase transition can happen by eliminating the energy gap of the insulator and generating the WP connection length from zero on.

II. THEORY OF OFF-RESONANT IRRADIATION EFFECT ON SOLID MEDIA

When a material is subjected by the irradiation of an electromagnetic field, the electromagnetic field can be described by its vector potential

$$\mathcal{A}(t) = \boldsymbol{A}_R \cos\omega t + \boldsymbol{A}_I \sin\omega t, \tag{1}$$

where ω is the angular frequency of light, t is the time, and $\boldsymbol{A}_R$ and $\boldsymbol{A}_I$ are the real and imaginary parts of the complex vector potential amplitude, say, $\boldsymbol{A} = \boldsymbol{A}_R + i\boldsymbol{A}_I$ (both $\boldsymbol{A}_R$ and $\boldsymbol{A}_I$ are vectors and they are orthogonal). The electromagnetic wave is assumed to propagate parallel or antiparallel to the direction of $\boldsymbol{A}_R \times \boldsymbol{A}_I$ and the positive propagation is assumed for convenience. The irradiation effect can be included into the k-space Hamiltonian of the material, $H(\boldsymbol{k})$, by means of the Peierls substitution $\boldsymbol{k} \to \boldsymbol{k} + \mathcal{A}$ (the electron charge e and the reduced Planck constant $\hbar$ are set to be units to simplify the notations) [55,56], where $\boldsymbol{k}$ is the wave vector. If the irradiation can be viewed as perturbation, we can expand the Hamiltonian up to the second order of $\mathcal{A}$ as

$$\begin{aligned}\tilde{H} &= H(\boldsymbol{k} + \mathcal{A}) \\ &= H(\boldsymbol{k}) + \mathcal{A}\cdot\nabla H(\boldsymbol{k}) + \tfrac{1}{2}(\mathcal{A}\cdot\nabla)^2 H(\boldsymbol{k}),\end{aligned} \tag{2}$$

with ∇ being the gradient operator in k space. Inserting the definition of $\mathcal{A}$ in Eq. (1) into the above equation, we have

$$\begin{aligned}\tilde{H} = H &+ \boldsymbol{A}_R\cdot\nabla H\ \cos\omega t + \boldsymbol{A}_I\cdot\nabla H \sin\omega t \\ &+ \tfrac{1}{2}(A_R\cos\omega t\nabla_R + A_I\sin\omega t\nabla_I)^2 H,\end{aligned} \tag{3}$$

where ∇_μ with $\mu = R, I$ is the k-space gradient along the direction of $\boldsymbol{A}_\mu$. After omitting harmonic components of frequency 2ω in the bracket square, the first and second order Hamiltonians caused by the Peierls substitution are

$$\begin{aligned}H^{(1)} &= \boldsymbol{A}_R\cdot\nabla H\ \cos\omega t + \boldsymbol{A}_I\cdot\nabla H\ \sin\omega t, \\ H^{(2)} &= \tfrac{1}{4}\left(A_R^2\nabla_R^2 H + A_I^2\nabla_I^2 H\right).\end{aligned} \tag{4}$$

The total time dependent Hamiltonian, up to the second order perturbation and base frequency, is thus

$$\tilde{H}(t) = H + H^{(1)}(t) + H^{(2)}. \tag{5}$$

One can see that the electromagnetic field induces a static correction and a harmonic perturbation to the unirradiated system.

The periodic driven system can be expressed as the Floquet Hamiltonian in energy space [24–27]. We keep only zero- and one-photon processes and the Floquet Hamiltonian is truncated to be

$$H_F = \begin{pmatrix} \mathcal{H}_{0,0} - \omega & \mathcal{H}_{-1,0} & 0 \\ \mathcal{H}_{0,-1} & \mathcal{H}_{0,0} & \mathcal{H}_{0,1} \\ 0 & \mathcal{H}_{1,0} & \mathcal{H}_{0,0} + \omega \end{pmatrix}, \tag{6}$$

where $\mathcal{H}_{m,m'}$ with $m, m' = 0, \pm 1$ is the harmonic component of the time dependent Hamiltonian $\tilde{H}$ with the frequency $(m - m')\omega$ and is defined by

$$\mathcal{H}_{m,m'} = \frac{1}{T}\int_0^T \tilde{H}\, e^{i(m'-m)\omega t} dt, \tag{7}$$

with $T = 2\pi/\omega$ being the driving period. Folding the Floquet Hamiltonian into the zero photon subspace, we have the effective Hamiltonian

$$H_{\text{eff}} = \mathcal{H}_{0,0} + \sum_{m=\pm 1} \mathcal{H}_{0,m} \frac{1}{E - (\mathcal{H}_{0,0} + m\omega)} \mathcal{H}_{m,0}, \tag{8}$$

where $\mathcal{H}_{0,0} = H + H^{(2)}$ is the time average of $\tilde{H}$ and the second term describes the correlation effect induced by an electron emitting a photon and reabsorbing it so as to return to the initial state. We reexpress $\mathcal{H}_{m,m+1}$ as V, and so $\mathcal{H}_{m+1,m}$ as V^+. In the limit of infinite ω, the effective Hamiltonian is reduced to

$$\begin{aligned} H_{\text{eff}} &= H + H^{(2)} + \frac{[V^+, V]}{\omega} \\ &= H + H^{(2)} + H_\omega. \end{aligned} \tag{9}$$

In the equation, $H^{(2)}$ and H_ω are both of the second order of $\mathcal{A}$ but have different physical originations. The former stems from the time-average effect of the perturbation [see the second line of Eq. (3)], while the latter is induced by the emission and reabsorption of photons, which is inverse proportional to the frequency. According to the first line of Eq. (4), one can easily obtain

$$V = \frac{1}{T}\int_0^T H^{(1)} e^{i\omega t} dt = \frac{1}{2} \boldsymbol{A} \cdot \nabla H. \tag{10}$$

Note that vector potential $\boldsymbol{A}$ is a complex vector; it can describe either linearly or elliptically polarized irradiation. For the linear polarization, $\boldsymbol{A}$ is real, and because ∇H is Hermitian, we have $[V^+, V] = 0$, so the linear polarized irradiation cannot induce any effect in H_ω.

For the elliptically or circularly polarized cases, $\boldsymbol{A}$ has nonzero imaginary part and H_ω is calculated to be

$$H_\omega = \frac{iA_R A_I}{\omega} [\nabla_R H, \nabla_I H]. \tag{11}$$

For linear polarized illumination, we have $A_R = 0$ and so $H_\omega = 0$, consistent with our assertion before. Assuming the illumination is applied in the direction of the unit vector $\boldsymbol{n}$, the above equation can be transformed as

$$H_\omega = \frac{A_R A_I}{\omega} \boldsymbol{D} \cdot \boldsymbol{n}, \tag{12}$$

where $\boldsymbol{D}$ is a Hermit vector defined by

$$\boldsymbol{D} = i(\nabla H \times \nabla H). \tag{13}$$

Substituting $H^{(2)}$ in Eq. (4) and H_ω in Eq. (12) into Eq. (9), we have the effective Hamiltonian to include the irradiation effect, which reads

$$H_{\text{eff}} = H + \frac{A_R A_I}{\omega} \boldsymbol{D} \cdot \boldsymbol{n} + \frac{1}{4}\left(A_R^2 \nabla_R^2 H + A_I^2 \nabla_I^2 H\right). \tag{14}$$

The effective Hamiltonian is general and independent of materials. One can find that the last term does not vanish if the Hamiltonian has k^2 or higher power of k terms and cannot be ignored because the off-resonant theory requires a large frequency limit. For linearly polarized irradiation ($A_I = 0$), the equation is reduced to $H_{\text{eff}} = H + A_R^2 \nabla_R^2 H/4$.

III. MULTIFOLD WEYL SEMIMETALS UNDER CIRCULARLY POLAR IRRADIATION

The minimal bipartite Hamiltonian of a Weyl semimetal with a pair of multifold WPs can be written as [57–59]

$$\begin{aligned} H &= v k_+^N \sigma_+ + v k_-^N \sigma_- + \left(k^2 - k_w^2\right)\sigma_z \\ &= \begin{pmatrix} k^2 - k_w^2 & v k_+^N \\ v k_-^N & k_w^2 - k^2 \end{pmatrix}, \end{aligned} \tag{15}$$

where N is a positive integer to indicate the Chern number of one WP, σ_α ($\alpha = x, y, z$) are Pauli matrices, $2k_w$ is the distance between the two WPs, k is the magnitude of wave vector $\boldsymbol{k}$, and v is a positive parameter of the dimension of k^{2-N} to balance the dimension between the matrix elements. In the equation, the notations $k_\pm = k_x \pm i k_y$ and $\sigma_\pm = (\sigma_x \pm i\sigma_y)/2$ are used. The WP locations are $\boldsymbol{K}_W = (0, 0, \pm k_w)$, which can be deduced by means of the zero energy condition.

In this paper, we only consider the circularly polarized irradiation, say $|A_R| = |A_I| = A_0$, so the effective Hamiltonian in Eq. (14) turns out to be

$$\begin{aligned} H_{\text{eff}} &= H + \tfrac{A_0^2}{\omega} \boldsymbol{D} \cdot \boldsymbol{n} + \tfrac{A_0^2}{4} \nabla_\perp^2 H \\ &= h_+ \sigma_+ + h_- \sigma_- + h_z \sigma_z, \end{aligned} \tag{16}$$

where $\nabla_\perp^2 = \nabla_R^2 + \nabla_I^2$ means the k-space Laplace operator in the plane perpendicular to the light propagation. In the equation, A_0^2/ω and A_0^2 mark the effect of H_ω and $H^{(2)}$, respectively. We rearrange the Hamiltonian as in the second line, in which h_z is real and $h_+ = h_-^+$ is a complex coefficient, to help us analyze the WP positions. The components of $\boldsymbol{D}$ can be straight calculated from (15) and they are

$$\begin{aligned} D_x &= 4N v k_z (k_+^{N-1}\sigma_+ + k_-^{N-1}\sigma_-), \\ D_y &= 4iN v k_z (k_+^{N-1}\sigma_+ - k_-^{N-1}\sigma_-), \\ D_z &= -4N v (k_+^N \sigma_+ + k_-^N \sigma_-) + 2N^2 v^2 k_\rho^{2N-2} \sigma_z, \end{aligned} \tag{17}$$

where $k_\rho = (k_x^2 + k_y^2)^{1/2}$.

Because the energy dispersion of the Hamiltonian is determined by $E^2 = |h_z|^2 + |h_+|^2$, the locations of WPs under the irradiation can be found out by letting

$$\begin{aligned} h_+ &= 0, \\ h_z &= 0. \end{aligned} \tag{18}$$

To achieve this, the expression of $\boldsymbol{D} \cdot \boldsymbol{n}$ and $\nabla_\perp^2 H$ for different illumination direction has to be specified.

A. Light illuminating in z direction

When the irradiation is applied along the z direction, $\boldsymbol{A}_R$ and $\boldsymbol{A}_I$ lie in the x-y plane, and we obtain

$$\begin{aligned} \boldsymbol{D} \cdot \boldsymbol{n} &= \chi D_z, \\ \nabla_\perp^2 H &= 4\sigma_z, \end{aligned} \tag{19}$$

where $\chi = \pm 1$ indicates the light propagates parallel (antiparallel) to the z axis. Inserting the above results into Eq. (16), the coefficients of σ_+ and σ_z in the effective Hamiltonian are calculated to be

$$h_+ = v k_+^N \left(1 - 4\chi N \frac{A_0^2}{\omega}\right),$$
$$h_z = k^2 - k_w^2 + 2\chi N^2 v^2 \frac{A_0^2}{\omega} k_\rho^{2N-2} + A_0^2. \tag{20}$$

The former tells $k_+ = 0$, say, $k_x = 0$ and $k_y = 0$, which means the WPs are always on the z axis, and the latter determines the WP positions on the axis.

When $N = 1$, one can find that $k_\rho^0 = 0^0$ appears in the second line of Eq. (20). We check the calculation of D_z in Eq. (17) and conclude that $k_\rho^0 = 1$ should be adopted here. In this situation, the pair of WPs are located at

$$\boldsymbol{K}_W = \left(0, 0, \pm\sqrt{k_w^2 - A_0^2\left(1 + \chi \frac{2v^2}{\omega}\right)}\right). \tag{21}$$

The WP connection length is a function of both A_0 and ω. The irradiation changes the WP connection length and the rate of change is different for illuminating along the z axis positively or negatively. For positive incidence, when the irradiation intensity reaches $A_0 = k_w/(1 + 2v^2/\omega)^{1/2}$, the WP connection length decreases to zero and the system undergoes a phase transition from Weyl semimetal to insulator. For negatively applied irradiation, the phase transition takes place at another irradiation intensity $A_0 = k_w/(1 - 2v^2/\omega)^{1/2}$. The $+z$ direction is the easy direction to induce the phase transition. Specially, if $\omega < 2v^2$, a negatively applied irradiation causes the WP connection length to be longer and such a phase transition cannot happen. The elongation of the WP connection means the irradiation can induce the reverse phase transition—the transition from an insulator to a Weyl semimetal. If we replace k_w with ik_w in Eq. (15), $k^2 - k_w^2$ is changed to be $k^2 + k_w^2$ and the Hamiltonian describes an insulator, which is identical to the Hamiltonian used in Ref. [31]. Now k_w is a parameter to determine not the WP positions but the energy gap $2k_w^2$. According to Eq. (20), the energy gap under irradiation is $2k_w^2 - 2A_0^2(2v^2/\omega - 1)$. When the irradiation intensity reaches $A_0 = \sqrt{k_w^2/(2v^2/\omega - 1)}$, the energy gap vanishes and the reverse phase transition occurs.

Figures 2(a) and 2(b) show the WP connection length as a function of A_0 for $N = 1$ at different ω. When A_0 increases, the distance decreases from its initial value $2k_w$ unless the irradiation is applied negatively and $\omega < 2v^2$. When the irradiation approaches its criterion intensity, the distance decreases to zero. At infinite ω limit, the critical intensity is $A_0 = k_w$, regardless of whether the irradiation is applied positively or negatively. Figures 2(c) and 2(d) show the phase boundaries between Weyl semimetal and insulator in A_0-ω^{-1} space. The vertical axis is set to be ω^{-1} to allow us to observe the phase transitions at large ω. There always is a phase transition happening for any value of ω when the positively applied irradiation increases, while when the irradiation is negatively applied, the transition is absent for large ω^{-1} (or small ω, explicitly, $\omega < 2v^2$).

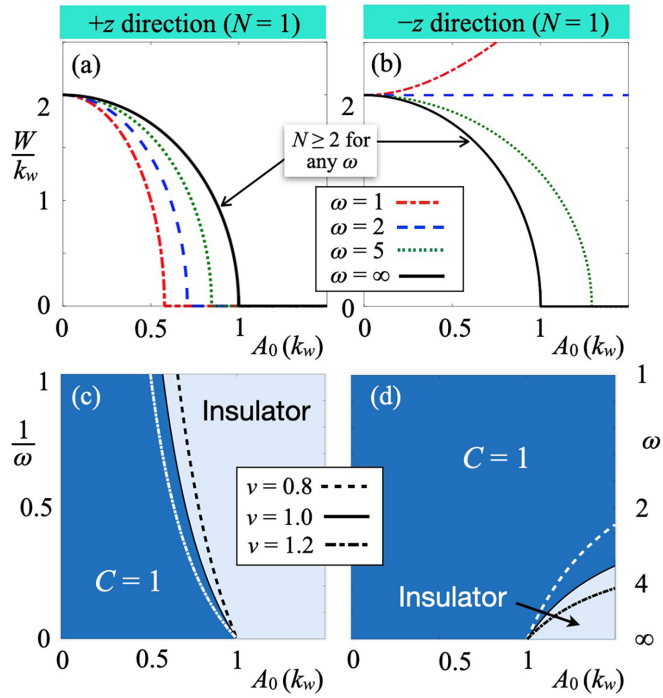

FIG. 2. Light illuminating along the z direction for $N = 1$. Upper panels: Weyl point connection length W as a function of A_0 for different ω (in units of k_w) at $v = 1$ in Eq. (15). Lower panels: phase boundaries for different v.

For the cases of $n \geqslant 2$, because of the constraint $k_+ = 0$ ($k_\rho = 0$), the WP positions are

$$\boldsymbol{K}_w = \left(0, 0, \pm\sqrt{k_w^2 - A_0^2}\right). \tag{22}$$

Interestingly, the positions are independent of N. In the equation, A_0^2/ω does not appear, which means H_ω has no effect on the WP moving and the moving is purely caused by $H^{(2)}$, and the equation possesses the only irradiation parameter A_0 and is irrelevant with ω, χ, and v. When the irradiation intensity reaches $A_0 = k_w$, the phase transition between multifold Weyl semimetal and insulator occurs. The irradiation can only shorten the WP connection, which means the reverse phase transition cannot take place for $N \geqslant 2$ cases. The WP connection length as a function of A_0 is just that for the $N = 1$ case at infinite ω limit [see Eq. (21)], as shown in Figs. 2(a) and 2(b).

B. Light illuminating in x direction

When the irradiation is applied along the x direction, the vectors $\boldsymbol{A}_R$ and $\boldsymbol{A}_I$ span in the y-z plane and we have

$$\boldsymbol{D} \cdot \boldsymbol{n} = \chi D_x,$$
$$\nabla_\perp^2 H = 4\sigma_z - vN(N-1)(k_+^{N-2}\sigma_+ + k_-^{N-2}\sigma_-), \tag{23}$$

where $\chi = \pm 1$ indicates the light is propagating parallel (antiparallel) to the x axis. Substituting the results in the above equation into Eq. (16), we have the coefficients h_+ and h_z in the effective Hamiltonian,

$$h_+ = v\left[k_+^N + 4\chi \frac{A_0^2}{\omega} N k_z k_+^{N-1} - \frac{A_0^2}{4} N(N-1) k_+^{N-2}\right], \tag{24}$$

$$h_z = k^2 - k_w^2 + A_0^2. \tag{25}$$

The equation is universal for any value of N.

When $N = 1$, the material possesses a pair of singlet WPs, the last term in h_+ in the above equation vanishes, and the constraint $h_+ = 0$ results in

$$(k_x + ik_y) + 4\chi \frac{A_0^2}{\omega} k_z = 0. \tag{26}$$

The imaginary part of the equation leads to $k_y = 0$, which means the WPs are on the k_x-k_z plane. The real part brings

$$\frac{k_x}{k_z} = -4\chi N \frac{A_0^2}{\omega}, \tag{27}$$

where N is preserved because the expression will be used later for values of N other than $N = 1$. The equation describes a line in the k_x-k_z plane (referred to as the tilting line in the following). The constraint $h_z = 0$ accompanied with $k_y = 0$ results in

$$k_x^2 + k_z^2 = k_w^2 - A_0^2. \tag{28}$$

The equation defines a circle (referred to as the node circle in the following), on which the WPs locate, with radius $(k_w^2 - A_0^2)^{1/2}$ in the k_x-k_z plane. The intersections between the tilting line and the nodal circle are the WP positions under the irradiation. When the light is applied positively or negatively along the x direction, the tilting line is rotated and deviated from the z axis counterclockwise or clockwise and, simultaneously, the node circle radius shrinks.

Figure 3(a) illustrates the trajectory of WPs moving in the k_x-k_z plane for the case of $N = 1$ when the irradiation increases from zero on. The WPs are initialed at $(0, \pm k_w)$ and the tilting line overlaps with the k_z axis. When the irradiation is turned on, the tilting line is rotating away from the k_z axis, the node circle is shrinking, and the intersections between the line and the circle are moving in the k_x-k_z plane. First, the tilting line rotates rapidly and the node circle shrinks slowly, so the intersection movement is almost tangent. Following, the line rotating is slowed down, the circle shrinking becomes fast, and the intersections move nearly radically. Because of the alternative change rates between the tilting line and the node circle, the trajectory of a WP pair is an S path. When the irradiation increases, the WPs start their travel from the two ends of the S path and move along and finally joint with each other at the middle point and cancel out there. The distance between the WPs as a function of A_0, which is shown in Fig. 3(b), is irrelevant with the shape of the trajectory curve, but is simply determined by the node circle radius. A Weyl semimetal to insulator transition occurs when the circle radius decreases to zero, say, at irradiation intensity $A_0 = k_w$.

If $N = 2$, the medium is a doublet Weyl semimetal and the constraint $h_+ = 0$ tells

$$(k_x + ik_y)^2 + 8\chi \frac{A_0^2}{\omega} k_z (k_x + ik_y) - \frac{A_0^2}{4} N(N-1) = 0. \tag{29}$$

The imaginary of the equation also results in $k_y = 0$. Applying it to the other constraint $h_z = 0$, we find that the WPs are on the circle defined in Eq. (28). The real part of the above equation brings a new constraint relation,

$$k_x^2 + 8\chi \frac{A_0^2}{\omega} k_z k_x - \frac{A_0^2}{4} N(N-1) = 0. \tag{30}$$

The equation defines a hyperbolic curve with two asymptotic lines. One asymptotic line is the tilting line described in

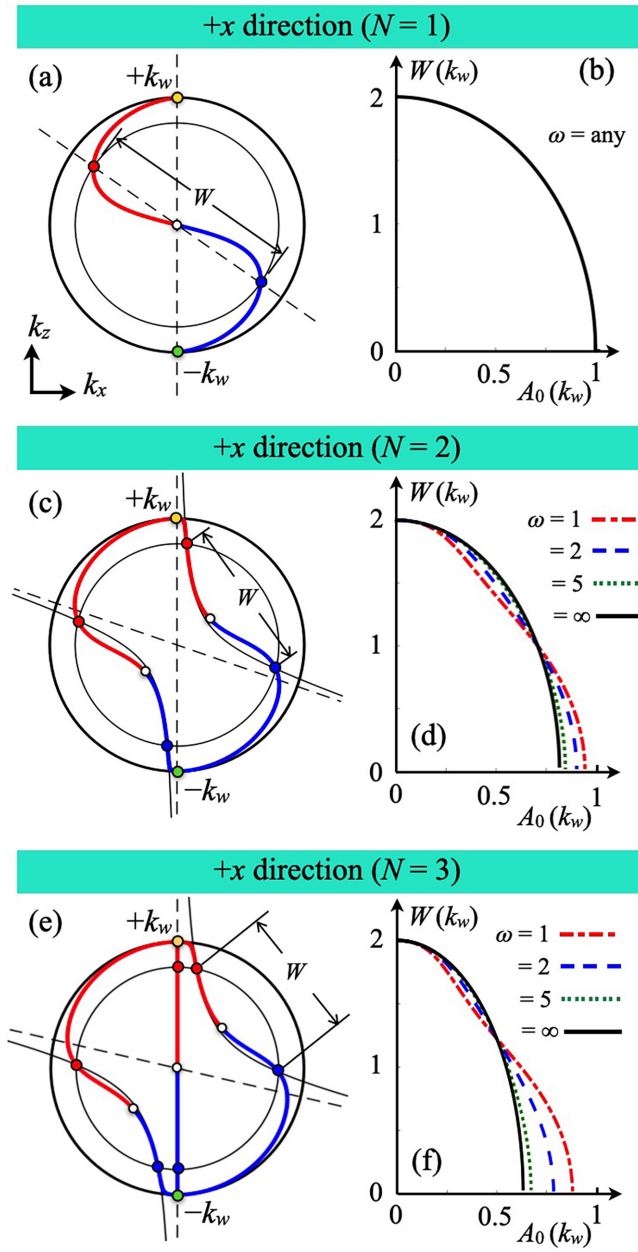

FIG. 3. Light illuminating along the x direction. Left panels: trajectories of Weyl points (WPs) moving in the k_x-k_z plane when A_0 increases. The outer and inner circles are the node circles defined in Eq. (28) for $A_0 = 0$ and $A_0 = 0.6k_w$, respectively. The thin solid curves are the hyperbolic curves at $A_0 = 0.6k_w$. The red and blue filled dots mark the intersections between the node circles and hyperbolic curves, which are the locations of the WPs for $A_0 = 0.6k_w$. The empty dots are the locations at which the WP pairs are gapped out. Right panels: distance between the WP pair canceled out first as a function of A_0 for different ω (in units of k_w). In all panels, $v = 1$ is adopted.

Eq. (27) in which $N = 2$ should be adopted now; the other is $k_x = 0$. Since the WPs are on the k_x-k_z plane, the latter asymptotic line is the k_z axis, which is not changed when the material is illuminated.

Figure 3(c) demonstrates the split WP trajectories of a doublet Weyl semimetal under irradiation. The two branches hyperbolic curve interacts with the node circle at four points that are the locations of the WPs. The illumination split each doublet WP into two singlet WPs. If the irradiation intensity increases, the circle becomes smaller, the tilting line rotates away, the hyperbolic curve changes correspondingly, and the intersections move and leave their tracks in the k_x-k_z plane. When the hyperbolic curve is detached from the circle, a phase transition between doublet Weyl semimetal and insulator takes place. Because the shape of the hyperbolic curve depends on the parameter ω, the critical intensity is a function of ω. Figure 3(d) shows the WP distance as a function of A_0 at different ω. At the infinite ω limit, the critical intensity takes the smallest value and is worked out to be $A_0 = k_w/[1 + N(N-1)/4]^{1/2}$, which is approximately $0.82k_w$ for $N = 2$.

When $N \geqslant 3$, the constraint $h_+ = 0$ leads to

$$k_+^{N-2}\left[k_+^2 + 4\chi N\frac{A_0^2}{\omega}k_z k_+ - \frac{A_0^2}{4}N(N-1)\right] = 0. \quad (31)$$

Apart from k_+^{N-2}, the rest of the equation is the same as Eq. (29), so its imaginary part results in $k_y = 0$ too, and its real part describes a new hyperbolic curve (because N is new) with two asymptotic lines implied by Eqs. (27) and the k_z axis. For each multifold WP, two singlet WPs are exfoliated from it and locate at the intersections between the hyperbolic curve and the node circle defined in Eq. (28), and a residual $(N-2)$-fold WP remains. The residual multifold WP position is indicated by the $(N-2)$-fold root of the equation, $k_+^{N-2} = 0$, which is to say that it lies at one of the intersections between the k_z axis and the node circle. as indicated in Fig. 3(e). When the irradiation intensity increases, the tilting line rotates and the node circle shrinks. Each WP pair exfoliated draws a trajectory branch and the residual pair runs on the k_z axis. At a critical intensity, the node circle is separated from the hyperbolic curve, the two pairs of exfoliated WPs are gapped out, and a phase transition from N-fold to $(N-2)$-fold Weyl semimetal takes place. At infinite ω limit, the critical intensity $A_0 = k_w/[1 + N(N-1)/4]^{1/2}$, the same expression as before but with different value of N, is $0.63k_w$ for $N = 3$. When the intensity reaches $A_0 = k_w$, the node circle radius decreases to zero and another phase transition, the phase transition from the $(N-2)$-fold Weyl semimetal to insulator, happens whatever value N takes. Figure 3(f) shows the distance between WPs in one pair as a function of A_0. The critical intensity is smaller than that of $N = 1$ and $N = 2$ cases and is the smallest at the infinite ω limit.

Figures 4(a) through 4(c) show the phase diagrams of multifold Weyl semimetals in A_0-ω^{-1} space. The phase boundary for single-fold Weyl media and insulator is simply a vertical line $A_0 = k_w$, but that between doublet Weyl medium and insulator is deviated from the vertical line apparently near the large ω end. When $N \geqslant 3$, a new phase region of $(N-2)$-fold Weyl semimetal arises. The N-fold Weyl semimetal cannot transit to insulator without experiencing the intermediate phase. The boundaries between the original phase and its adjacent phase (the phase that the medium is turned into first when A_0 increases) for different N are exhibited all in one in Fig. 4(d).

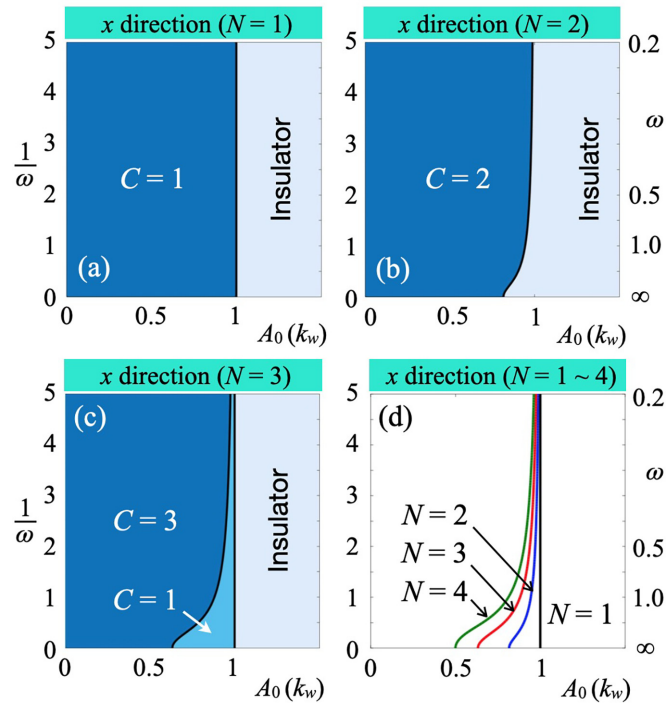

FIG. 4. Phase diagrams for light illuminating along the x direction. (a)–(c) Phase diagrams for Weyl semimetals of fold $N = 1, 2, 3$. (d) Boundaries between the phase of multifold Weyl semimetal and the adjacent phase of matter for $N = 1 \sim 4$.

The above results are obtained for the illumination along the x axis. If the light propagates in another direction in the x-y plane, the split WPs will distribute and move in the $\boldsymbol{n}$-k_z plane and the obtained conclusions remain valid. If one rotates the light beam in the x-y plane, the plane of the split WPs laying will change following the incident rotation. When the incidence is rotated by angle π, the rotation of the tilting line is reversed indeed, which is the same effect as reversing χ, consistent with our afore results.

IV. REMARKS AND CONCLUSIONS

The time average perturbation $H^{(2)}$ and the photon emission-absorption effect H_ω play different roles when the irradiation is applied and they are featured in the equations by A_0^2 and A_0^2/ω, respectively. The topological phase transitions of matter are caused by $H^{(2)}$ because it determines the radius of the node circle and H_ω only justifies the manner of WP approaching by controlling the tilting line. Among all types of multifold Weyl semimetals, the singlet Weyl semimetal is the most special one to respond to the irradiation. It is the only material in which the effect of H_ω is involved in the phase transitions of matter [both the terms A_0^2 and A_0^2/ω appear in Eq. (21)]. The irradiation along the WP connection does not split multifold WPs. It not only can shorten the WP connection

as usual but also can elongate it. The elongation effect implies that the reverse phase transition can be induced. Such reverse transition cannot happen in other Weyl semimetals. It was believed that the photon emission-absorption effect plays the key role for the phase transitions of Weyl semimetals [41]; indeed, the viewpoint is only valid for one special value of N, say, $N = 1$.

The effect of irradiation reversal is equivalent to that of reversing the circular polarization or changing the chirality of the Weyl Hamiltonian, say, exchanging k_+ and k_- in Eq. (15). In some realistic singlet Weyl semimetals, for example, in Na_3Bi [60], WP chirality is bounded with electron spin, so the irradiation reversal can also be regarded as spin flipping in these materials and electrons of opposite spins have different response to the irradiation, as reported in Ref. [33]. When the light illuminates in the direction of WP connection, the WP connection lengths of different spins are modified with different rates. It is possible that one spin species falls in the insulator state and the other spin species stays in the Weyl semimetal state, as discussed in Ref. [45].

The irradiation perpendicular to the WP connection splits the N-fold WP pair into three pairs—two singlet pairs and the remaining $(N-2)$-fold pair. The three pairs are scattered in the plane formed by the WP connection and the light propagation direction. The two singlet pairs leave two S paths when the irradiation increases, move along their S paths from the path ends, and will be canceled out simultaneously at a critical irradiation intensity depending on N. In the meantime, the WPs of the remaining pair approach each other straight along the WP connection line and are finally gapped out at another irradiation intensity irrelevant of N. In the multifold Weyl semimetal irradiated, there exist three topological phases of matter, say, N-fold Weyl semimetal, $(N-2)$-fold and insulator, and the transitions between them can be realized by changing the irradiation intensity. After two singlet WPs are exfoliated from each multifold WP, the remaining WPs are still multifold if $N > 3$ and cannot be resolved furthermore even increasing the irradiation intensity. This is because the off-resonant theory is a second order perturbation one. If higher order perturbation is taken into account, more pairs of WPs will be exfoliated, but the split will be less remarkable and is not considered in this paper.

We only give the analytical calculations for irradiation along z and x directions. If the irradiation is applied in other directions, the intermediate cases can be understood quantitatively by turning on the irradiation along the $+z$ direction and rotating it counterclockwise by a full round. When the irradiation appears, the WP connection shrinks on the k_z axis. When irradiation is rotated away, each WP is split and deviates from the k_z axis and the deviation is most notable at the rotation angle 90°. Proceeding the rotation, the deviation decreases and the split WPs merge at the k_z axis at the rotation angle 180°. If the rotation is going on, the WPs will resplit and are deviated reversely, and the WPs recover their locations when the full round of rotation is completed. During the rotation, all the split WPs shift on the node circle for $N \geqslant 2$, while, for $N = 1$, the WP connection changes its length, which is shortest at zero rotation angle and longest at the angle 180°.

ACKNOWLEDGMENTS

This work was supported by the National Natural Science Foundation of China under Grants No. 12174121 and No. 12274146 and the Guangdong Basic and Applied Basic Research Foundation under Grant No. 2023B1515020050.

[1] N. P. Armitage, E. J. Mele, and A. Vishwanath, Weyl and Dirac semimetals in three-dimensional solids, Rev. Mod. Phys. **90**, 015001 (2018).

[2] P. Narang, C. A. C. Garcia, and C. Felser, The topology of electronic band structures, Nat. Mater. **20**, 293 (2021).

[3] B. Q. Lv, T. Qian, and H. Ding, Experimental perspective on three-dimensional topological semimetals, Rev. Mod. Phys. **93**, 025002 (2021).

[4] S.-M. Huang, S.-Y. Xu, I. Belopolski, C.-C. Lee, G. Chang, T.-R. Chang *et al.*, New type of Weyl semimetal with quadratic double Weyl fermions, Proc. Natl. Acad. Sci. USA **113**, 1180 (2016).

[5] B. Singh, G. Chang, T.-R. Chang, S.-M. Huang, C. Su, M.-C. Lin *et al.*, Tunable double-Weyl Fermion semimetal state in the $SrSi_2$ materials class, Sci. Rep. **8**, 10540 (2018).

[6] Q. Liu and A. Zunger, Predicted realization of cubic Dirac Fermion in quasi-one-dimensional transition-metal monochalcogenides, Phys. Rev. X **7**, 021019 (2017).

[7] N. B. M. Schröter, S. Stolz, K. Manna, F. de Juan, M. G. Vergniory, J. A. Krieger *et al.*, Observation and control of maximal Chern numbers in a chiral topological semimetal, Science **369**, 179 (2020).

[8] T. Dubček, C. J. Kennedy, L. Lu, W. Ketterle, M. Soljačić, and H. Buljan, Weyl points in three-dimensional optical lattices: Synthetic magnetic monopoles in momentum space, Phys. Rev. Lett. **114**, 225301 (2015).

[9] N. Han, J. Liu, Y. Gao, K. Zhou, and S. Liu, Topological phase transitions and Weyl semimetal phases in chiral photonic metamaterials, New J. Phys. **24**, 053052 (2022).

[10] W. Song, S. Wu, C. Chen, Y. Chen, C. Huang, L. Yuan, S. Zhu, and T. Li, Observation of Weyl interface states in non-Hermitian synthetic photonic systems, Phys. Rev. Lett. **130**, 043803 (2023).

[11] E. Lustig and M. Segev, Topological photonics in synthetic dimensions, Adv. Opt. Photon. **13**, 426 (2021).

[12] H. Ge, X. Ni, Y. Tian, S. K. Gupta, M.-H. Lu, X. Lin, W. D. Huang, C. T. Chan, and Y. F. Chen, Experimental observation of acoustic Weyl points and topological surface states, Phys. Rev. Appl. **10**, 014017 (2018).

[13] V. Peri, M. Serra-Garcia, R. Ilan, and S. D. Huber, Axial-field-induced chiral channels in an acoustic Weyl system, Nat. Phys. **15**, 357 (2019).

[14] K. S. Novoselov, A. K. Geim, S. V. Morozov, D. Jiang, Y. Zhang, S. V. Dubonos *et al.*, Electric field effect in atomically thin carbon films, Science **306**, 666 (2004).

[15] A. H. Castro Neto, F. Guinea, N. M. R. Peres, K. S. Novoselov, and A. K. Geim, The electronic properties of graphene, Rev. Mod. Phys. **81**, 109 (2009).

[16] M. Ezawa, Photoinduced topological phase transition and a single Dirac-cone state in silicene, Phys. Rev. Lett. **110**, 026603 (2013).

[17] G. Usaj, P. M. Perez-Piskunow, L. E. F. F. Torres, and C. A. Balseiro, Irradiated graphene as a tunable Floquet topological insulator, Phys. Rev. B **90**, 115423 (2014).

[18] P. M. Perez-Piskunow, G. Usaj, C. A. Balseiro, and L. E. F. F. Torres, Floquet chiral edge states in graphene, Phys. Rev. B **89**, 121401(R) (2014).

[19] A. Kundu, H. A. Fertig, and B. Seradjeh, Floquet-engineered valleytronics in Dirac systems, Phys. Rev. Lett. **116**, 016802 (2016).

[20] M. Yang, Z.-J. Cai, R.-Q. Wang, and Y.-K. Bai, Topologically trivial and nontrivial edge bands in graphene induced by irradiation, Phys. Lett. A **380**, 2836 (2016).

[21] L. E. F. Foa Torres, P. M. Perez-Piskunow, C. A. Balseiro, and G. Usaj, Multiterminal conductance of a Floquet topological insulator, Phys. Rev. Lett. **113**, 266801 (2014).

[22] A. Kundu, H. A. Fertig, and B. Seradjeh, Effective theory of Floquet topological transitions, Phys. Rev. Lett. **113**, 236803 (2014).

[23] M. S. Rudner and N. H. Lindner, Band structure engineering and non-equilibrium dynamics in Floquet topological insulators, Nat. Rev. Phys. **2**, 229 (2020).

[24] J. Cayssol, B. Dóra, F. Simon, and R. Moessner, Floquet topological insulators, Phys. Status Solidi **7**, 101 (2013).

[25] M. Bukov, L. D'Alessio, and A. Polkovnikov, Universal high-frequency behavior of periodically driven systems: from dynamical stabilization to Floquet engineering, Adv. Phys. **64**, 139 (2015).

[26] U. D. Giovannini and H. Hübener, Floquet analysis of excitations in materials, J. Phys. Mater. **3**, 012001 (2020).

[27] T. Oka and S. Kitamura, Floquet engineering of quantum materials, Annu. Rev. Condens. Matter Phys. **10**, 387 (2019).

[28] N. Sirica, P. P. Orth, M. S. Scheurer, Y. M. Dai, M.-C. Lee, P. Padmanabhan *et al.*, Photocurrent-driven transient symmetry breaking in the Weyl semimetal TaAs, Nat. Mater. **21**, 6266 (2022).

[29] Y. Tanaka and M. Mochizuki, Dynamical phase transitions in the photodriven charge-ordered Dirac-electron system, Phys. Rev. Lett. **129**, 047402 (2022).

[30] S. S. Dabiri, H. Cheraghchi, and A. Sadeghi, Light-induced topological phases in thin films of magnetically doped topological insulators, Phys. Rev. B **103**, 205130 (2021).

[31] Q. Yang and Q. Tong, Light-induced topological phases in two-dimensional gapped Dirac materials, Phys. Rev. B **106**, 115406 (2022).

[32] D. Zhang, H. Wang, J. Ruan, G. Yao, and H. Zhang, Engineering topological phases in the Luttinger semimetal α-Sn, Phys. Rev. B **97**, 195139 (2018).

[33] H. Hübener, M. A. Sentef, U. De Giovannini, A. F. Kemper, and A. Rubio, Creating stable Floquet-Weyl semimetals by laser-driving of 3D Dirac materials, Nat. Commun. **8**, 13940 (2017).

[34] C. K. Chan, Y. T. Oh, J. H. Han, and P. A. Lee, Type-II Weyl cone transitions in driven semimetals, Phys. Rev. B **94**, 121106(R) (2016).

[35] A. Narayan, Tunable point nodes from line-node semimetals via application of light, Phys. Rev. B **94**, 041409(R) (2016).

[36] K. Taguchi, D.-H. Xu, A. Yamakage, and K. T. Law, Photovoltaic anomalous Hall effect in line-node semimetals, Phys. Rev. B **94**, 155206 (2016).

[37] T. Deng, B. Zheng, F. Zhan, J. Fan, X. Wu, and R. Wang, Photoinduced Floquet mixed-Weyl semimetallic phase in a carbon allotrope, Phys. Rev. B **102**, 201105(R) (2020).

[38] R. Chen, B. Zhou, and D.-H. Xu, Floquet Weyl semimetals in light-irradiated type-II and hybrid line-node semimetals, Phys. Rev. B **97**, 155152 (2018).

[39] B. Dey and T. K. Ghosh, Floquet topological phase transition in the α-$\mathcal{T}_3$ lattice, Phys. Rev. B **99**, 205429 (2019).

[40] A. Kumar, M. Rodriguez-Vega, T. Pereg-Barnea, and B. Seradjeh, Linear response theory and optical conductivity of Floquet topological insulators, Phys. Rev. B **101**, 174314 (2020).

[41] R. Wang, B. Wang, R. Shen, L. Sheng, and D. Y. Xing, Floquet Weyl semimetal induced by offresonant light, Europhys. Lett. **105**, 17004 (2014).

[42] S. Sajad Dabiri, H. Cheraghchi, and A. Sadeghi, Floquet states and optical conductivity of an irradiated two-dimensional topological insulator, Phys. Rev. B **106**, 165423 (2022).

[43] M. Rodriguez-Vega, A. Kumar, and B. Seradjeh, Higher-order Floquet topological phases with corner and bulk bound states, Phys. Rev. B **100**, 085138 (2019).

[44] Z.-M. Wang, R. Wang, J.-H. Sun, T.-Y. Chen, and D.-H. Xu, Floquet Weyl semimetal phases in light-irradiated higher-order topological Dirac semimetals, Phys. Rev. B **107**, L121407 (2023).

[45] X.-S. Li, C. Wang, M.-X. Deng, H.-J. Duan, P.-H. Fu, R.-Q. Wang, L. Sheng, and D. Y. Xing, Photon-induced Weyl half-metal phase and spin filter effect from topological Dirac semimetals, Phys. Rev. Lett. **123**, 206601 (2019).

[46] Y. H. Wang, H. Steinberg, P. Jarillo-Herrero, and N. Gedik, Observation of Floquet-Bloch states on the surface of a topological insulator, Science **342**, 453 (2013).

[47] F. Mahmood, C.-K. Chan, Z. Alpichshev, D. Gardner, Y. Lee, P. A. Lee *et al.*, Selective scattering between Floquet-Bloch and Volkov states in a topological insulator, Nat. Phys. **12**, 306310 (2016).

[48] A. Huamán, L. E. F. Foa Torres, C. A. Balseiro, and G. Usaj, Quantum Hall edge states under periodic driving: A Floquet induced chirality switch, Phys. Rev. Res. **3**, 013201 (2021).

[49] J. W. McIver, B. Schulte, F.-U. Stein, T. Matsuyama, G. Jotzu, G. Meier *et al.*, Light-induced anomalous Hall effect in graphene in off-resonant and resonant regions, Nat. Phys. **16**, 38 (2020).

[50] S. Aeschlimann, S. A. Sato, R. Krause, M. Chávez-Cervantes, U. De Giovannini, H. Hübener *et al.*, Survival of Floquet-Bloch states in the presence of scattering, Nano Lett. **12**, 5028 (2021).

[51] Z. Yan and Z. Wang, Floquet multi-Weyl points in crossing-nodal-line semimetals, Phys. Rev. B **96**, 041206(R) (2017).

[52] M. Ezawa, Photoinduced topological phase transition from a crossing-line nodal semimetal to a multiple-Weyl semimetal, Phys. Rev. B **96**, 041205(R) (2017).

[53] M. Umer, R. W. Bomantara, and J. Gong, Nonequilibrium hybrid multi-Weyl semimetal phases, J. Phys. Mater. **4**, 045003 (2021).

[54] K. Plekhanov, G. Roux, and K. Le Hur, Floquet engineering of Haldane Chern insulators and chiral bosonic phase transitions, Phys. Rev. B **95**, 045102 (2017).

[55] R. Peierls, On the theory of diamagnetism of conduction electrons, Z. Phys. **80**, 763 (1933).

[56] G. H. Wannier, Dynamics of band electrons in electric and magnetic fields, Rev. Mod. Phys. **34**, 645 (1962).

[57] G. Xu, H. Weng, Z. Wang, Xi Dai, and Z. Fang, Chern semimetal and the quantized anomalous Hall effect in $HgCr_2Se_4$, Phys. Rev. Lett. **107**, 186806 (2011).

[58] C. Fang, M. J. Gilbert, X. Dai, and B. A. Bernevig, Multi-Weyl topological semimetals stabilized by point group symmetry, Phys. Rev. Lett. **108**, 266802 (2012).

[59] W. C. Silva, W. N. Mizobata, J. E. Sanches, L. S. Ricco, I. A. Shelykh, M. de Souza, M. S. Figueira, E. Vernek, and A. C. Seridonio, Topological charge Fano effect in multi-Weyl semimetals, Phys. Rev. B **105**, 235135 (2022).

[60] Z. K. Liu, B. Zhou, Y. Zhang, Z. J. Wang, H. M. Weng, D. Prabhakaran, S.-K. Mo, Z. X. Shen, Z. Fang, X. Dai, Z. Hussain, and Y. L. Chen, Discovery of a three-dimensional topological Dirac semimetal, Na_3Bi, Science **343**, 864 (2014).